J. Fluid Mech. (2014), *vol.* 751, *pp.* 106–120. © Cambridge University Press 2014
doi:10.1017/jfm.2014.289

Electrohydrodynamics of particle-covered drops

Malika Ouriemi† and Petia M. Vlahovska

School of Engineering, Brown University, Providence, RI 02906, USA

(Received 10 December 2013; revised 16 May 2014; accepted 20 May 2014;
first published online 16 June 2014)

We experimentally investigate the effect of surface-absorbed colloidal particles on the dynamics of a leaky dielectric drop in a uniform DC electric field. Depending on the particle polarizabilty, coverage and the electrical field intensity, particles assemble into various patterns such as an equatorial belt, pole-to-pole chains or a band of dynamic vortices. The particle structuring changes droplet electrohydrodynamics: under the same conditions where a particle-free drop would be a steady oblate spheroid, the belt can give rise to unsteady behaviours such as sustained drop wobbling or tumbling. Moreover, particle chaining can be accompanied by prolate drop deformation and tip-streaming.

Key words: colloids, drops, electrohydrodynamic

1. Introduction

A neutral droplet placed in a uniform electric field deforms into an axisymmetric ellipsoid under weak field conditions $Ca \ll 1$, where the capillary number $Ca = a\varepsilon E_0^2/\gamma$ compares the stresses due to electric field with intensity E_0 and the interfacial tension, γ, acting on a drop with radius a. Weakly conducting (leaky dielectric) fluids exhibit either prolate or oblate drop shapes depending mainly on the ratio of conductivities, $R = \sigma_d/\sigma_s$ and permittivities $S = \varepsilon_s/\varepsilon_d$ of the drop, 'd', and suspending, 's', fluids (Taylor 1966); see Lac & Homsy (2007) for a recent review on this classic problem. Drop deformation is accompanied by axisymmetric straining flow, whose direction depends on RS, e.g. from the pole towards the equator if $RS < 1$, see figure 1. In stronger electric fields, in the case $RS < 1$ the flow also acquires a rotational component (Ha & Yang 2000; Salipante & Vlahovska 2010; He, Salipante & Vlahovska 2013), which gives rise to steady drop tilt (figure 1*c*) or various unsteady responses such as shape oscillations or drop tumbling (Sato *et al.* 2006; Salipante & Vlahovska 2013).

Colloidal particles have a strong tendency to adsorb at interfaces and are often used to stabilize emulsions (Binks 2002; Aveyard, Binks & Clint 2003). The behaviour of particle-covered drops in electric field has received surprisingly little attention despite some intriguing reports about particle redistribution along the drop interface in uniform AC fields (Nudurupati *et al.* 2008, 2009, 2010) or structuring in uniform DC fields (Dommersnes *et al.* 2013). The latter study showed that in the case $RS < 1$, particles initially randomly distributed at the surface (figure 1*d*), form a

† Permanent address: IFPEN, Solaize, BP 3, 69360, France. Email address for correspondence: malika.ouriemi@ifpen.fr

https://doi.org/10.1017/jfm.2014.289 Published online by Cambridge University Press

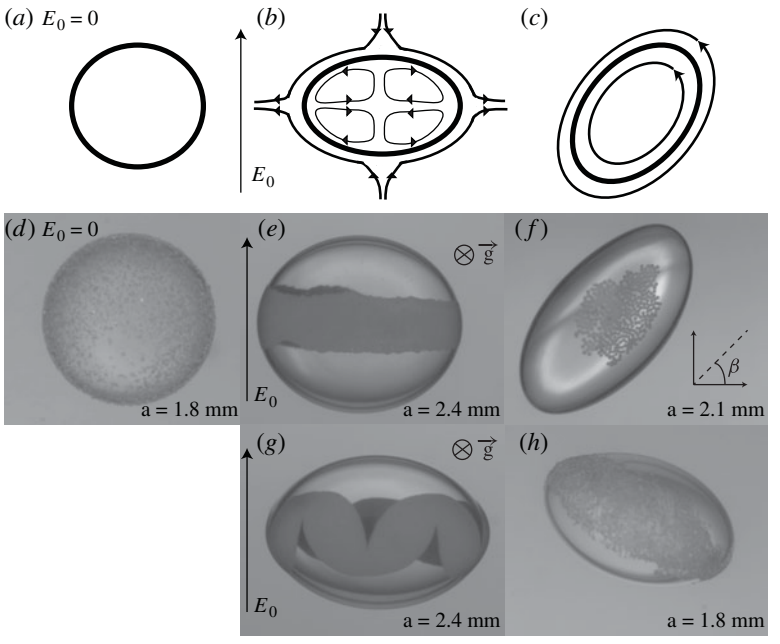

FIGURE 1. Drop response to a uniform DC electric field for $RS < 1$. (*a*,*d*) In the absence of electric field, the drop is spherical and particle distribution is random. (*b*,*c*) Sketch of the particle-free drop shape and flow streamlines in weak fields (axisymmetric oblate spheroid and straining flow) and in strong fields, where the drop is tilted and the flow has a rotational component. (*d–h*) Snapshots of particle-covered drops at different electrical field strengths.

'belt' around the equator as the drop deforms into an oblate shape, see figure 1(*e*). This is an expected consequence of the straining electrohydrodynamic flow. However, other peculiar (and seemingly random) patterns were also observed such as a band of counter-rotating vortices (see figure 1*g*) or a partial chaining dubbed 'pupil' (Dommersnes *et al.* 2013). In stronger DC fields, we find that convection by the rotational flow can result in either particles orbiting along closed streamlines or clustering (see figure 1*f*). We also discovered new behaviours such as wobbling and tumbling drops, see figure 1(*h*) and the supplementary material available at http://dx.doi.org/10.1017/jfm.2014.289. In this work we conduct a systematic study of a particle-covered drop placed in a uniform DC field in the $RS < 1$ regime and classify the various behaviours into phase diagrams. While keeping the drop and suspending fluids the same, we vary the particle size, shape, conductivity and coverage in order to correlate particle structuring to particle properties and electric field strength.

2. Materials and experimental procedure

The suspending fluid is castor oil with viscosity $\mu_s = 0.69$ Pa s, dielectric constant $\varepsilon_s = 4.7\varepsilon_0$, conductivity $\sigma_s = 3.8 \times 10^{-11}$ S m^{-1} and density $\rho_s = 962$ kg m^{-3} (Alfa Aesar). The drop fluid is silicon oil with $\mu_d = 0.05$ Pa s, $\varepsilon_d = 2.8\varepsilon_0$, $\sigma_d = 3.6 \times 10^{-12}$ S m^{-1}, $\rho_d = 963.5$ kg m^{-3} (UTC). Accordingly, $R = 0.1$, $S = 1.7$ and the viscosity ratio $\lambda = 0.07$. The interfacial tension is 4.5 mN m^{-1} (Salipante & Vlahovska 2010). The permittivity and the conductivity were measured using a

https://doi.org/10.1017/jfm.2014.289 Published online by Cambridge University Press

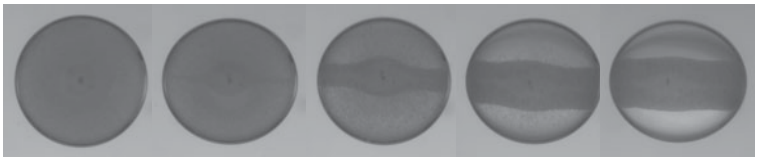

FIGURE 2. Preparing the particle-covered drop. Initially the particles are suspended in the drop, as seen by the uniform dark colour. Upon the application of an electric field, the particles migrate to the interface and accumulate at the belt. The fact that the particles are leaving the bulk is seen by the clearing of the drop fluid (above and below the belt).

Shape	Type	ρ_p (kg m^{-3})	radius r (μm)	Conductivity (S m^{-1})	Supplier
Random	Aluminum (Al)	2600	1.5, 12, 100	3.8×10^{3}	Atlantic equipment
Spherical	Al coated ceramic (Ac)	850	6	3.8×10^{1}	Accumet materials
Spherical	Glass (G)	2200	5, 8.5, 50	1×10^{-10}	Corpuscular/Cospheric
Random	Fingerprint (F)	2080	0.5	—	Lynn Peavey Co.
Spherical	Polyethylene (Pe)	1000	50	3.2×10^{-24}	Cospheric
Spherical	PMMA (P)	1200	8.5	1×10^{-17}	Cospheric
Random	Silver (Si)	8900	1.5	6.3×10^{7}	Atlantic equipment
Spherical	Si coated glass (Sg)	2500	8.5	6.3×10^{5}	Cospheric

TABLE 1. Particle characteristics. Conductivity for G spheres was furnished by the supplier, other conductivities correspond to the conductivity of the bulk material. No value was obtained for the fingerprint.

dielectric constant meter and a conductivity meter from Scientifica. The viscosity was specified by the company–provider. The characteristics of the particles are summarized in table 1.

A uniform electric field is created in a parallel-plate chamber filled with castor oil. The chamber has a similar design as that used by Salipante & Vlahovska (2010): the walls are 7 cm $\times$ 10 cm brass electrodes separated by a 4.5 cm gap. DC fields up to 16 kV cm^{-1} are generated using a voltage amplifier and a DC power supply. A drop of silicon oil with suspended microparticles is injected into the middle of the electrical chamber. The particles are driven to the interface by the application of an electric pulse (the duration and strength of which depend on the type of microparticles, e.g. for glass spheres of radius 5 μm, $E_0 = 1.6$ kV cm^{-1} and pulse duration is 4 min). During the initial pulse, the electrohydrodynamic flow inside the drop brings the particles to the interface, while the flow at the interface drags the particles toward the equator, see figure 2. Once all particles are trapped at the drop interface (in a belt), the electric field is turned off. The drop is then manually moved around in order to destroy any particle structures, erase any memory of the initial pulse and randomize the particle distribution on the drop surface.

https://doi.org/10.1017/jfm.2014.289 Published online by Cambridge University Press

In the actual experiment, electric field is applied and drop behaviour is recorded for approximately 3 min. After each recording, the electrical field is turned off and the drop is moved back to its initial position. This action removes any particle structures. The experiment is repeated for a different electric field strength. The surface concentration of particles, φ, is defined as the percentage of the drop surface covered by particles (which includes the space between particles) once the particles are brought together in the belt. We measure φ at very low electrical fields, $E_0 < 0.6$ kV cm^{-1}, to minimize particle compaction.

Owing to the small density difference between the drop and the continuous phase, the drop sediments on the time scale of the experiment (3 min). The drops considered in our study range from 1 to 5 mm in diameter, resulting in terminal velocities from 0.001 to 0.03 mm s^{-1}. The microparticles also experience buoyancy, however their estimated terminal velocities are tens to hundreds of times smaller than the drop speed, with the exception of the large Al and Ac particles ($r \sim 100$ μm) which can reach 0.1 mm s^{-1}. These velocities are much smaller than the electrohydrodynamic flow, $v_e \sim a\varepsilon_s E_0^2/\mu_s \sim 1$ mm s^{-1} (at $E_0 = 1$ kV cm^{-1}), and hence the buoyancy effects should play a negligible role in determining the particle distribution under an electric field; the buoyancy force acting on the particles is much weaker than the electrohydrodynamic drag, see the online supplementary material for more details.

3. Results and discussion

3.1. *Droplet behaviour and particle structures*

Figure 3 summarizes drop behaviour and particle assemblies as a function of the field strength and particle conductivity for moderate coverage ($\varphi \sim 50\,\%$) and similar particle size (radius $r \sim 10$ μm). In weak fields, $Ca \leqslant 1$, the drop always deforms into an oblate spheroid and the particles accumulate at the equator forming a 'belt' (figure 3*a–c*). In stronger fields, three scenarios are observed. First, the belt can break into a regular sequence of counter-rotating assemblies of particles (resembling a 'sinusoid'), while drop shape and orientation are steady (figure 3*f*). Second, the belt stays stationary while the drop wobbles, namely its major axis oscillates around a direction perpendicular to the applied field (see figure 3*e* and the movies in the online supplementary material). Third, the particles form chains and the drop shape changes to a prolate ellipsoid. In this regime, the pole-to-pole chains of particles line up parallel to the electrical field (figure 3*d*). In very strong fields, the prolate drops covered with particle chains undergo tip streaming with the ejection of particles (see figure 3*g*) while the oblately deformed drops rotate (see figure 3*i*). In this case, the belt particles redistribute and can either entirely lose structure, or get partially ejected. In the latter case, the particles remaining on the surface form a cluster around the rotational axis (see figure 1*f*). In the particular case of aluminum particles with random shapes, the drop rotation mode is more peculiar: the belt structure is preserved, drop precesses and the particle belt is spinning around the drop major axis (see figure 3*h* and the movies in the supplementary material).

Figure 4 provides more details about how the particle shape and size affect the destabilization of the belt. Particles with high polarizability, i.e. highly conducting small particles or large particles with conductivity higher than the embedding fluids (such as silver-coated glass spheres, large glass spheres and large aluminum particles), never form a sinusoid but instead chain up. Spheres organize into regular chains parallel to the applied field direction (figure 4*e,j*), while random shaped particles

https://doi.org/10.1017/jfm.2014.289 Published online by Cambridge University Press

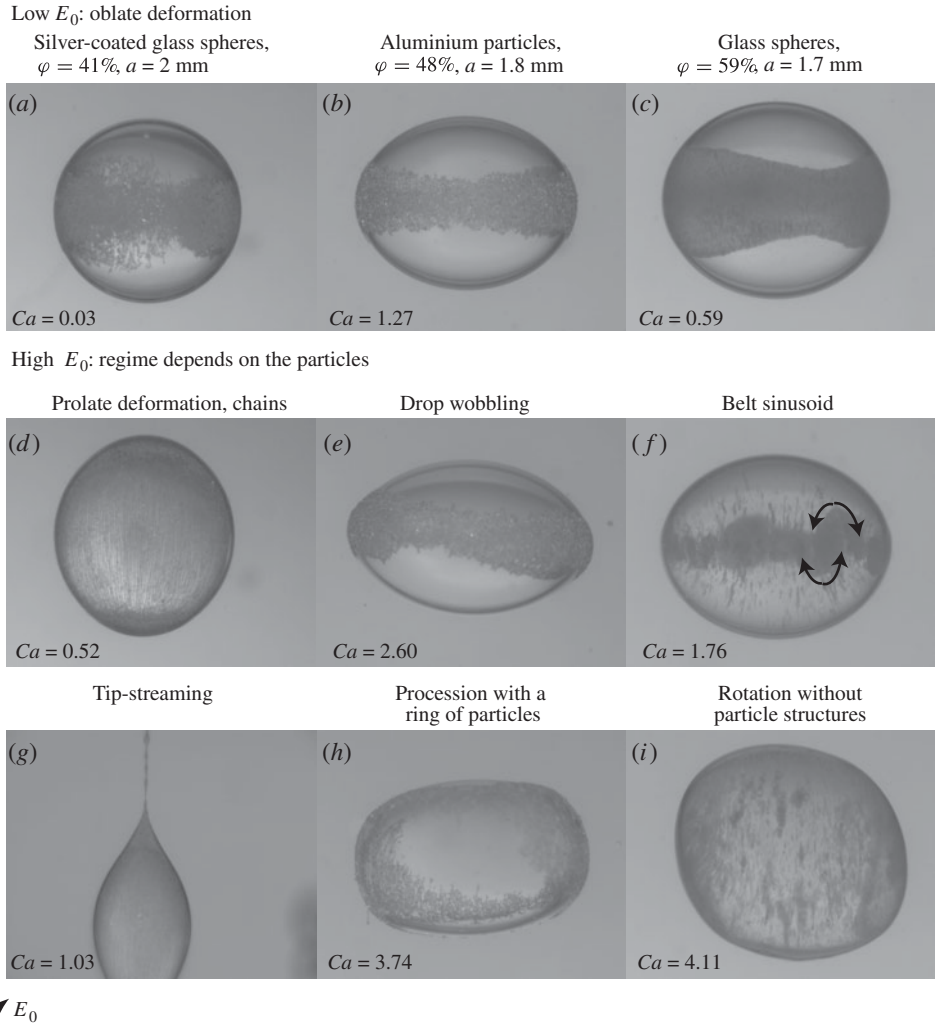

FIGURE 3. Drop shape and particles structures at increasing field strength Ca. Each column represents the same drop. The particle radius is approximately 10 μm. See the movies in the supplementary material.

form an irregular network (figure 4*a*,*i*). Particles with low polarizability (such as the low conducting PMMA, PE, fingerprint, small glass and very small aluminum particles) form a dynamic sinusoid (figure 4*b*,*c*,*d*,*g*,*h*,*k*). Drop wobbling is correlated with intermediate size ($r \sim 10$ μm) and conductivity (Al) particles with random shape (see figure 4*f*). Figure 4 behaviours are relatively insensitive to the coverage with the exception of the Ac spheres.

For this system (Ac), figure 5 illustrates the differences in drop behaviour due to particle coverage. Under the same field strength, a lower coverage results in a belt, while a higher coverage drop exhibits wobbling. Upon increase of the field strength, the lower coverage belt forms a dynamic sinusoid, while the higher coverage drop forms a static sinusoid characterized by no vortices. Further increase in the field

https://doi.org/10.1017/jfm.2014.289 Published online by Cambridge University Press

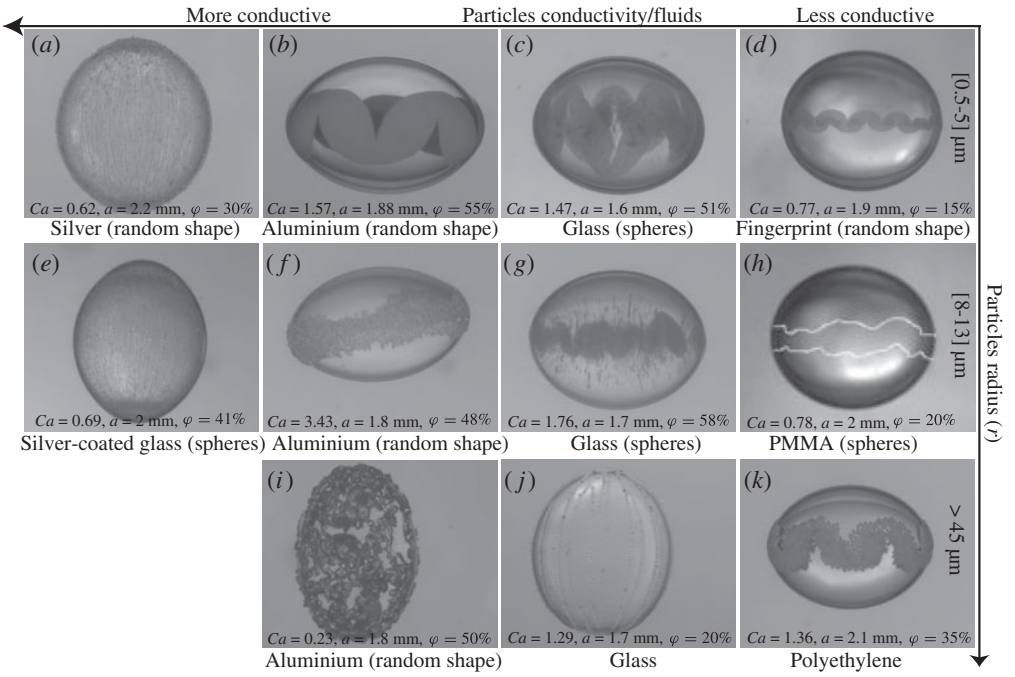

FIGURE 4. Dependence of the structure on particle properties.

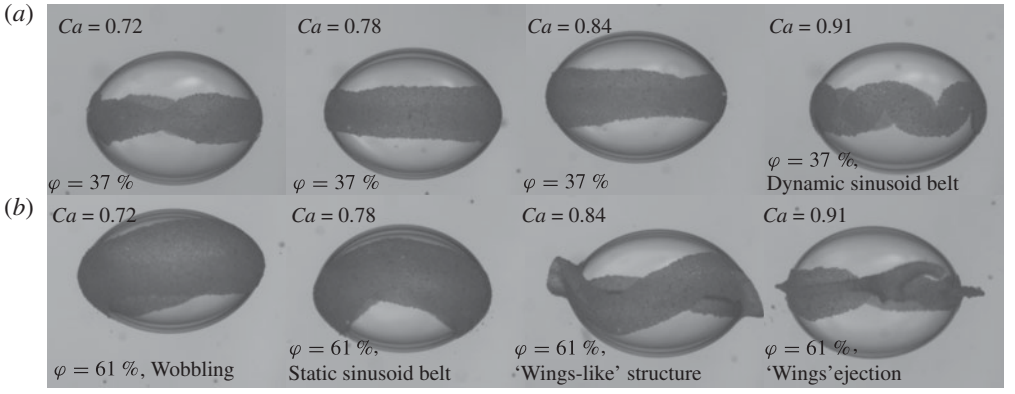

FIGURE 5. Effect of surface coverage on belt dynamics. A drop ($a = 2.2$ mm) covered with Ac spheres ($r = 6$ μm) with a surface coverage $\varphi = 37\,\%$ (*a*) and $\varphi = 61\,\%$ (*b*).

strength gives rise to a 'wing-like' structure, in which some of the particles are detached form the drop interface, and eventually get ejected.

The belt can also display some peculiar, previously unreported features. Increasing the field strength can lead to further destabilization of the structure resulting in vortices that periodically change orientation (swing), see figure 6(*a*). The structuring also appears to be history-dependent. Figure 6(*b*) shows the belt evolution upon turning on and off the field. During the first pulse (4 min) the belt forms a steady sinusoid with a 'wing-like' structure, which would have undergone ejection should the

https://doi.org/10.1017/jfm.2014.289 Published online by Cambridge University Press

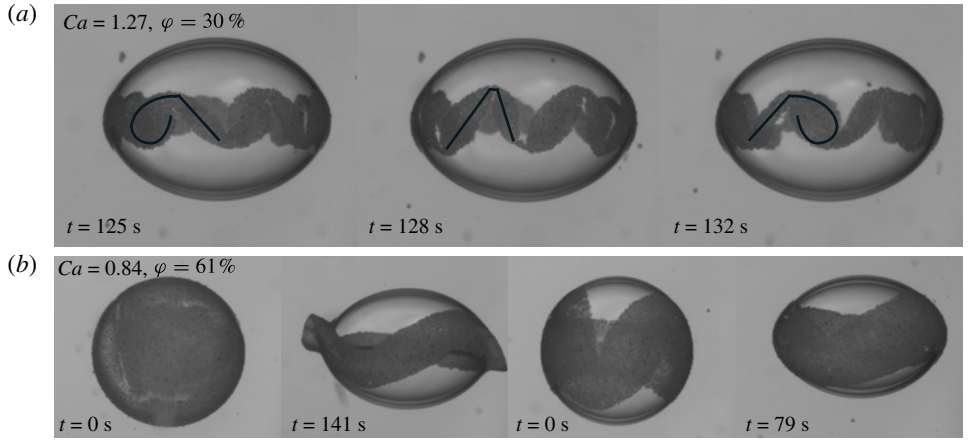

FIGURE 6. (*a*) 'Swinging' vortices: temporal evolution of a sinusoid for a drop ($a = 2.2$ mm) covered with Ac spheres ($r = 6$ μm) for $Ca = 1.27$ and $\varphi = 30\,\%$. The dark lines are added to guide the eye. (*b*) Effect of initial particle distribution on belt structure for a drop ($a = 2.2$ mm) covered with Ac spheres ($r = 6$ μm) for $Ca = 0.84$ and $\varphi = 61\,\%$.

field was slightly higher. When the field is turned off, the drop relaxes to a sphere but the belt remains. Upon application of a second pulse with the same strength the belt never forms wings, i.e. particle ejection is suppressed. So, the fact that the particles were already packed in a belt (i.e. initially structured) shifts the onset of particle ejection to stronger fields.

3.2. *Mechanisms*

The effect of particles on the overall drop deformation is illustrated in figure 7, where the experimental data are compared with the Taylor's linear theory with capillary number defined based on the clean drop interfacial tension

$$D = \frac{a_{\parallel} - a_{\perp}}{a_{\parallel} + a_{\perp}} = Ca \frac{9}{16S^2(2+R)^2} \left[S(R^2+1) - 2 + 3(RS-1)\frac{2\lambda+3}{5\lambda+5} \right]. \tag{3.1}$$

Intriguingly, the elongation of drops covered with variety of particles and coverages are well described by the Taylor law at much wider range of Ca compared to clean drops. For example, particle-covered drops can follow the linear law up to $Ca \sim 2.5$. In contrast, particle-free ('clean') drops begin to deviate from the Taylor law at $Ca \sim 0.5$.

The deviation from the Taylor law occurs at the onset of buckling or wobbling. Compared with the belt buckling, the onset of drop wobbling is observed at higher field strengths. The buckling onset is particle and coverage dependent: the lower the particle coverage, the lower the field strength required to form the sinusoid. This is expected as buckling should depend on the belt width. In contrast, the wobbling threshold seems to be coverage independent: drops covered with aluminum particles with $\varphi = 1$, 22 and 48 % all begin to wobble at about the same Ca. This finding suggests that in this case overall drop deformation and particle cohesion are the controlling factors.

https://doi.org/10.1017/jfm.2014.289 Published online by Cambridge University Press

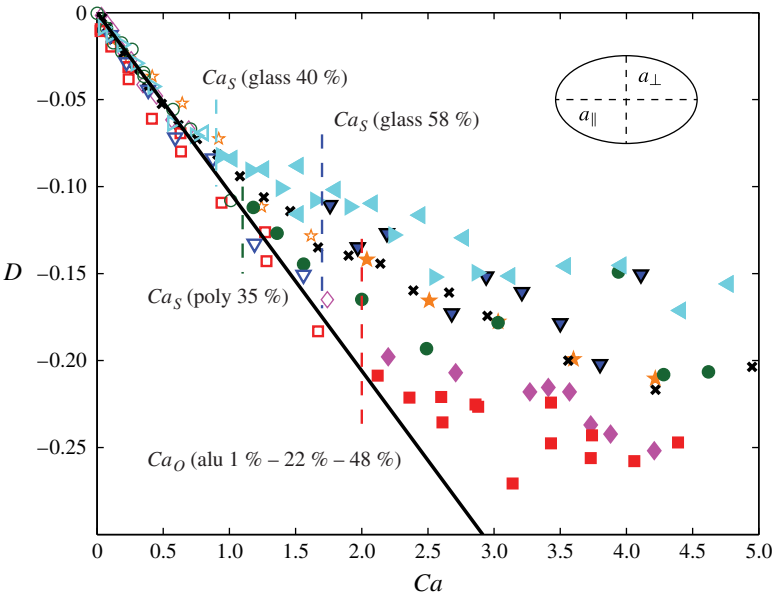

FIGURE 7. (Colour online) Deformation parameter D as a function of the capillary number. The symbol $\times$ corresponds to a 'clean' (particle-free) drop with $a = 2.2$ mm, the symbol $\circ$ corresponds to a drop covered with PE ($\varphi = 35\,\%$, $a = 2$ mm), the symbols $\bigstar$, $\square$ and $\diamond$ denote drops covered with Al with $\varphi = 1$, 22 and 48 % and $a = 1.9$, 2 and 1.8 mm, the symbols $\triangleleft$, $\triangleright$ and $\triangle$ correspond to drops covered with G with $\varphi = 38$, 40 and 59 % and $a = 1.8$, 1.6 and 1.7 mm. The filled symbols indicate that the drops experience wobbling or sinusoids. The solid line corresponds to the Taylor prediction (3.1).

3.2.1. *Belt dynamics*

The formation of the belt is driven by the electrohydrodynamic flow, which convects particles towards the equator. Particle also experience dielectrophoresis due to the nonuniform electric field along the drop interface but this effect is weaker. One can see this by comparing the magnitudes of the electrohydrodynamic and the dielectrophoretic velocities. The first can be estimated from the solution for the electrohydrodynamic flow around a spherical drop (Taylor 1966) $v_e \sim a\varepsilon_s E_0^2/\mu_s$. The dielectophoretic velocity is obtained by balancing the dielectrophoretic force and hydrodynamic drag $v_d \sim (\varepsilon_s r^3 K_{cm} E_0^2/a)/(\mu_s r)$, where $K_{cm} = (\sigma_p - \sigma_s)/(\sigma_p + 2\sigma_s)$ denotes the particle Clausius–Mossotti factor. Thus, $v_e/v_d \sim a^2/r^2 \gg 1$.

At this time, we can only speculate about the mechanism of the belt buckling and the formation of the dynamic vortices, see figure 8. It is possible that the electrohydrodynamic flow quickly jams particles in the belt, which then buckles when compressed by the surface tension acting to restore the spherical drop shape. Indeed the instability is observed at $Ca \geqslant 1$, where the flow time scale $t_e \sim \mu_s/\varepsilon_s E_0^2$ is shorter than the surface tension time scale $t_e \sim a\mu_s/\gamma$. Alternatively, it may be the electrohydrodynamic flow compressing the 'elastic' particle sheet that drives the buckling. The fact that the sheet is confined to the surface and it is essentially a granular material must play a role in its response. Once the belt is buckled the background electrohydrodynamic flow shears the particles and drives the vortices. However, if the particle cohesion is strong, e.g. due to compaction, strong dipole–dipole interactions, or jamming due to irregular shape, the flow may not be

https://doi.org/10.1017/jfm.2014.289 Published online by Cambridge University Press

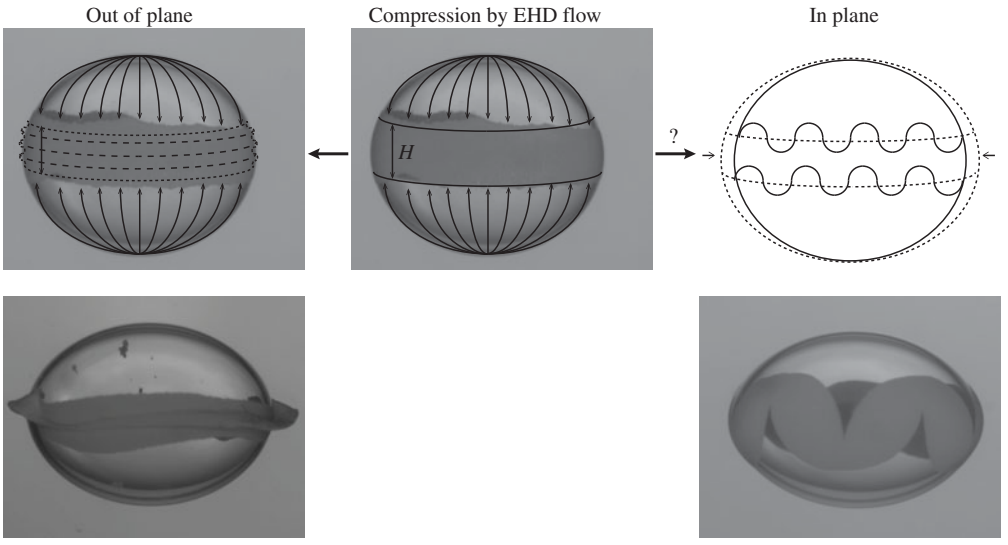

FIGURE 8. Sketch of the potential scenarios for 'out-of-plane' and 'in-plane' belt buckling.

able to put the particles in motion. As a result, the sinusoid would remain static which is indeed the case for high coverages, see figure 5(*b*) (second snapshot). Variation in the particle cohesion may also be responsible for the history-dependent belt dynamics seen in figure 6. Particles that are already packed in a belt resist removal from the drop surface, i.e. the formation of 'wings' and ejection.

Under compression, the density of particles at the interface increases and approaches jamming (Vella, Aussillous & Mahadevan 2004; Planchette, Lorenceau & Biance 2012). The compressive stress increases with the field strength leading to decrease in the belt width, see figure 9(*a*) and the supplementary material, however, the effect is not very strong. The decreased belt width correlates with higher particle compaction, which is seen in figure 9(*b*). The data shows that the particle area fraction φ_r, determined experimentally by visually counting the particles on the surface, is approaching random close packing in two dimensions $\varphi_{RCP} = 0.84$.

The compressed particle layer can undergo out-of-plane buckling instability forming wrinkles and folds (Vella *et al.* 2004; Pocivavsek *et al.* 2008). Cerda & Mahadevan (2003) showed that the balance of the foundation and bending energies leads to the selection of wrinkles of an intermediate wavelength $\Lambda \sim (B/K)^{1/4}$, where B is the bending rigidity of the particle layer and K is the stiffness due to an 'elastic substrate'; the amplitude of the wrinkles $\sim\Lambda$. For of a flat particle layer ('raft') residing on a fluid/fluid interface, the liquid buoyancy acts as the effective stiffness, thus $K = \Delta\rho g$; the bending rigidity is $B \sim Yh^3$ where $Y \sim \gamma/h$ is the Young's modulus and $h = 2r$ is the particle diameter (Vella *et al.* 2004). Hence, the wrinkle wavelength is $\Lambda_o \sim (\gamma h^2/\Delta\rho g)^{1/4} \sim 1$ mm (for $h = 10$ μm).

In our system, the particle layer resides on a curved interface, with radius of curvature set by the drop radius a. Buckling on any length scale on the drop surface costs energy $\sim\gamma/a^2$ (Finken & Seifert 2006) because the area of a surface element changes as it moves outwards or inwards. Accordingly, in our system for 'out-of-plane' buckling the surface tension dominates over gravity and $K \sim \gamma/a^2$.

https://doi.org/10.1017/jfm.2014.289 Published online by Cambridge University Press

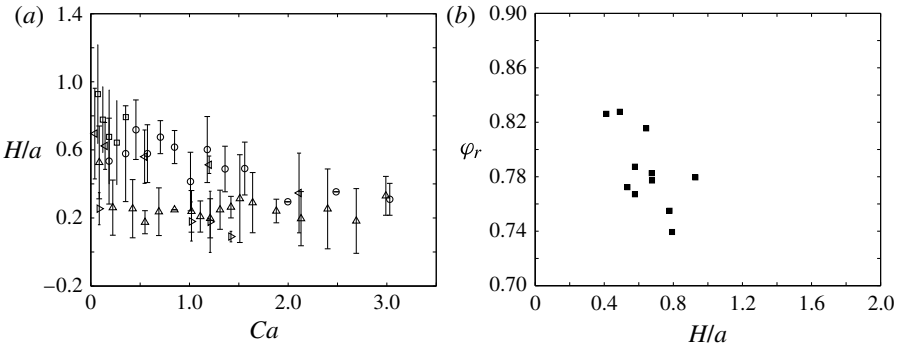

FIGURE 9. (*a*) Belt width (normalized by a) as a function of the capillary number for PE. The symbols □, ◁, ○, △ and ▷ correspond to drops covered with respectively $\varphi = 35\,\%$ ($Ca_S > 0.35$), $28\,\%$ ($Ca_S > 1.20$), $34\,\%$ ($Ca_S > 1$), $16.5\,\%$ ($Ca_S > 1.11$), and $8\,\%$ ($Ca_S > 0.08$). (*b*) Surface fraction φ_r in the belt for a coverage $\varphi = 35\,\%$ of polyethylene particles as a function of the belt width (normalized by a).

The wrinkle wavelength is $\Lambda_o \sim \sqrt{ah} \sim 0.1$ mm (for $h = 10$ μm). A more precise estimate using the expressions by Vella *et al.* (2004) shows that actually the wrinkle wavelength is of the order of the particle diameter and, hence, too short to be observable. However, in very strong fields and belt can fold due to stress focusing and this may be responsible for the wings, see figure 5(*b*) ($Ca = 0.84$).

In the studies of particle rafts, the particles cover the whole interface and buckling out of plane is the only possible response to compression. In our systems, the drop surface is only partially covered and the belt can buckle 'in-plane', remaining confined to the drop interface. The measured wavelength is shown in figure 10. It appears it is not sensitive to the field strength and increases with the belt width H, see also the supplementary material for additional data. The strong dependence on H is probably due to the energy cost for bending. The geometric constraint that the belt is confined to a surface with a radius of curvature a suggests a new variable, $\sqrt{aH}$. The experimental data for the sinusoid wavelength Λ is well described in terms of this scaling, as seen in figure 10(*b*), with the exception of the thin belts. This is likely due to the fact that a very thin belt, $H \ll a$, is not strongly affected by the drop curvature.

The mechanism of the in-plane buckling instability is not apparent at this time but it likely involves interplay between a destabilizing force (the electrohydrodynamic flow) and a restoring force (provided by the belt resistance to bending). Recasting the experimental data for belt states, stable and buckled, in terms of these two forces collapses the data on a phase-diagram with well-defined transition, see figure 11(*a*). Both forces are scaled by surface tension. The dimensionless bending stress is then $B/a^2\gamma$, where the bending rigidity B is determined following Vella *et al.* (2004) using the belt thickness, $B = YH^3/12(1-\nu^2)$, $Y = 2.82(\gamma/(2r))$ and $\nu = 1/\sqrt{3}$. The electrohydrodynamics stress is estimated from the Taylor solution at the location of the belt boundary $\theta_c = \theta(z = H/2)$ and $T_{el} = \varepsilon_d E_0^2(1 - RS)/(R+2)^2 \sin(2\theta_c)$. The dimensionless electrohydrodynamic stress is then $T_{el}a/\gamma$. Phase diagram with the same variables also provides good separation between the regimes of steady belted drops and wobbling/tumbling drops, see figure 11(*b*).

https://doi.org/10.1017/jfm.2014.289 Published online by Cambridge University Press

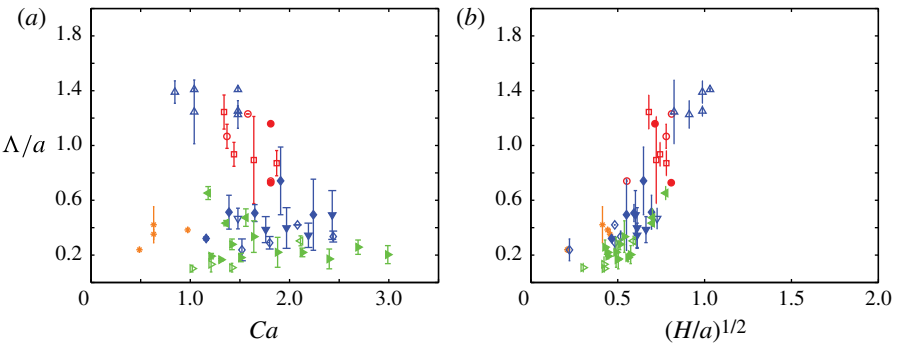

FIGURE 10. (Colour online) Wavelength Λ (normalized by the drop radius a) as a function of (a) the capillary number and (b) belt width $\sqrt{H/a}$. The $\square$ empty and filled symbols correspond to Ac-covered drops with $\varphi = 37$ and 61 %, respectively. The empty and filled $\circ$ symbols correspond to a Al-covered drop ($r = 1.5$ μm) with $\varphi = 54$ and 50 %, the symbols $\star$ to drops covered with F with $\varphi = 15$ %, the symbol $\triangle$ to drops covered with G ($r = 5$ μm, $\varphi = 51$ %). G-covered drops ($r = 8.5$ μm) with $\varphi = 38$, 40, 53, 58 and 59 % are represented by empty and filled $\diamond$ symbols, the filled symbol $\triangle$, the empty and filled symbols $\triangledown$. The empty and filled $\triangleright$ symbols and the empty and filled $\triangleleft$ symbols denote PE-covered drops with $\varphi = 8$, 16, 28 and 34 %.

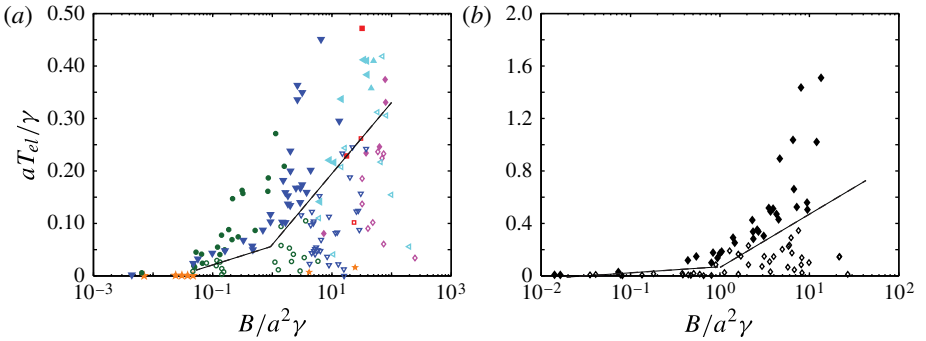

FIGURE 11. (Colour online) (a) Phase diagram for drops covered with low polarizability particles. The empty symbols correspond to drops with steady belts, while the filled symbols denote drops with buckled belts. The line is added to guide the eye. The symbol $\diamond$ denotes drops covered with Al ($r = 1.5$ μm, $\varphi = 54$ and 50 %), the symbol $\star$ denotes drops covered with F ($\varphi = 15$ %), the symbol $\square$ denotes drops covered with G ($r = 5$ μm, $\varphi = 51$ %), the symbol $\circ$ denotes drops covered with PE ($\varphi = 8$, 16, 28 and 34 %), the symbol $\triangledown$ denotes drops covered with G ($r = 7.5$ μm, $\varphi = 38$, 40, 53, 58 and 59 %) and the symbol $\triangleleft$ denotes drops covered with Ac ($\varphi = 37$ and 61 %). Drops with higher coverage of Ac ($\varphi = 61$ %) instead of belt buckling undergo drop wobbling (symbol $\triangle$). (b) Phase diagram for drops covered with intermediate polarizability particles Al ($r = 12$ μm, $\varphi = 1$, 22, 18 and 48 %). The filled symbols indicate that the drops experience oscillations. The line is added to guide the eye.

3.3. *Wobbling and tumbling*

'Wobbling' is characterized by small oscillations of the drop main axis while the particle equatorial ring remains nearly intact. The drop inclination relative to the

https://doi.org/10.1017/jfm.2014.289 Published online by Cambridge University Press

applied field direction is quantified by the angle β, see figure 1. Figure 12 complies the time evolution of β for different Ca and the same drop. Above $Ca = 2.6$, the drop long axis starts to swing. On the time scale of the observation, no clear period of the oscillation emerges. Above $Ca = 3.7$, the drop starts to 'tumble'. This behaviour is characterized by a steady periodic oscillation of β accompanied by rotation of the belt around the drop long axis, see figure 12(*b*). Increasing Ca widens the belt due to the appearance of chains (see $Ca = 4.4$ sequence). At even higher field strengths, the belt breaks into two rotating domains, see figure 1(*f*), and the drop adopts a steady tilt relative to the applied field direction.

Drop wobbling may be due to Quincke rotation, i.e. the appearance of electric torque above a threshold electric field. This phenomenon occurs for a drop with characteristic charge relaxation time larger than the surrounding fluid ($RS < 1$) (Jones 1984). In this case, the induced drop dipole is oriented in the opposite direction to the applied electric field. This configuration is unfavourable; it becomes unstable above a critical strength of the electric field and a perturbation in the dipole orientation creates a constant torque. In the case of a rigid sphere, this results in physical rotation of the particle known as Quincke rotation. The induced surface charges rotate with the particle, but at the same time the suspending fluid recharges the interface. The balance between charge convection by rotation and supply by conduction from the bulk results in continuous sphere spinning. The period of rotation is

$$T_Q = 2\pi t_{mw} \left(\frac{E^2}{E_Q^2} - 1 \right)^{-1/2} \tag{3.2}$$

where E_Q is the threshold electric field above which the rotation occurs and t_{mw} is the Maxwell–Wagner polarization time

$$E_Q^2 = \frac{2\sigma_s \mu_s \, (R+2)^2}{3\varepsilon_s \varepsilon_d (1 - RS)}, \quad t_{mw} = \frac{\varepsilon_d + 2\varepsilon_s}{\sigma_d + 2\sigma_s}. \tag{3.3a,b}$$

In our experiments, we find that the threshold electric field for wobbling $E_w/E_Q \sim 1$–1.5, close to the Quincke value. Moreover, the observed drop tumbling period of approximately 20 s is also close to the Quincke period (approximately 10 s), which is rather surprising considering that the drops in our experiment are ellipsoidal and a belt with different conductivity is present at their equator. Numerical simulations show that in DC fields a rigid ellipsoid cannot only align with the field but exhibit oscillations, precessing and tumbling (Cebers, Lemaire & Lobry 2002; Dolinsky & Elperin 2009). Particle-free droplets also display rotations however accompanied with large deformation, unlike the case here (Salipante & Vlahovska 2013). In our system, the belt retains its structure (probably due to strong particle cohesion) thereby constraining the drop shape during wobbling.

3.4. *Chains regime*

The prolate drop deformation probably originates from strong surface conduction (due to the presence of very conducting particles at the interface) which suppresses and even reverses the electrohydrodynamic flow. The formation of the chains is promoted by dipole–dipole interactions, which for spheres lead to attraction parallel to the electric field direction. Random shape particles, however, have anisotropic interactions, which result in the irregular structure.

https://doi.org/10.1017/jfm.2014.289 Published online by Cambridge University Press

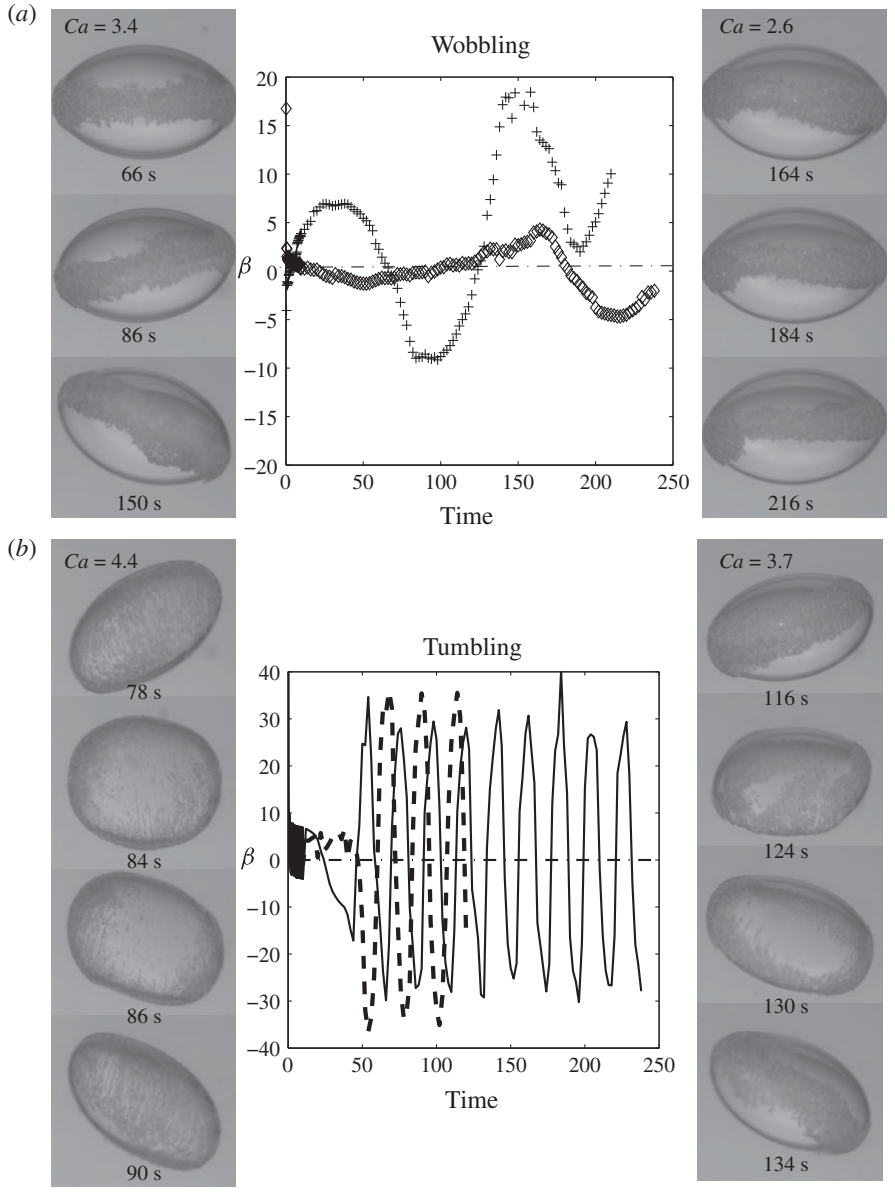

FIGURE 12. Evolution of the inclination of the drop, β, with time for wobbling (a) and tumbling drops (b) covered with Al particles ($r = 12$ μm). (a) The symbol $\diamond$ corresponds to $Ca = 2.6$, and $+$ to $Ca = 3.4$. (b) The solid line corresponds to $Ca = 4.1$ and the dashed line corresponds to $Ca = 4.4$.

The electric field leading to the formation of chains decreases with the particles conductivity, coverage and particle spacing. The latter depend on compaction, which in turns depends on field strength. As a result, a precise electric field threshold for the chains regime is difficult to define. Chains may form but not grow to cover the whole surface, see the supplementary material (this structure was called a 'pupil' by Dommersnes *et al.* (2013)). Moreover, figure 13 shows that in some cases particles

https://doi.org/10.1017/jfm.2014.289 Published online by Cambridge University Press

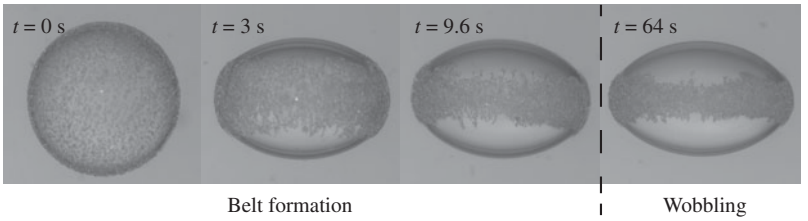

FIGURE 13. Temporal belt evolution for a drop covered with aluminum particles ($\varphi = 48\,\%$) for $Ca = 2.86$.

quickly chains after the application of the electric field, but the chains get broken and compacted at later times due to the compression by the electrohydrodynamic flow. This occurs when the dipole–dipole attractive forces are comparable to the electrohydrodynamic forces, which is the case of intermediate-polarizability or random-shaped particles.

Particle chaining may lead to increasing the belt width with the electric field strength (in contrast to the chain-free particle belts shown in figure 9). The belt widening, first reported as the 'pupil effect' by Dommersnes *et al.* (2013), was attributed solely to particles with intermediate conductivity by these authors. We find that any particles which are more conducting than the suspending fluids can display the pupil behaviour at some particle size and field strength. This effect is illustrated in the supplementary material with glass and silver-coated spheres, as examples of low- and high-conductivity particles, respectively.

4. Conclusions and outlook

We have experimentally studied the dynamics of colloidal particles adsorbed on a drop placed in a uniform DC electrical field. The fluid system consists of a silicon oil drop suspended in castor oil, both very weakly conducting liquids. A broad range of particle sizes, conductivities and shapes is explored. In weak electric fields, the electrohydrodynamic flow convects all particles towards the equator forming a 'belt'. In stronger electrical fields, the evolution of the belt depends on the particles characteristics and coverage. Belts formed by low polarizability particles break into a sequence of counter-rotating vortices of particles. The vortices themselves can undertow periodic changes in orientation. When dipole–dipole attraction becomes strong the particle chain and the drop experiences a prolate deformation and tip-streaming occur with ejection of particles. For non-spherical conductive particles, we observe a new regime with sustained oscillation of the drop inclination with respect to the applied field while the belt is stable. In this paper we focus on relatively low particle coverage. Higher coverage leads to other intriguing behaviours such as 'drum-like' drop shapes and implosion, see the supplementary material.

The diversity of particle patterns provides promising new ideas for directed assembly of particles at interfaces. Our findings open questions ranging from understanding the mechanism for particle organization to stability of Pickering emulsions. We hope our work will stimulate further research on the electrohydrodynamics of particles at interfaces.

Acknowledgements

This research was supported by NSF awards CBET-1117099 and CBET-1132614.

https://doi.org/10.1017/jfm.2014.289 Published online by Cambridge University Press

Supplementary movies and material

Supplementary movies and material are available at http://dx.doi.org/10.1017/jfm.2014.289.

REFERENCES

AVEYARD, R., BINKS, B. P. & CLINT, J. H. 2003 Emulsions stabilised solely by colloidal particles. *Adv. Colloid Interface Sci.* **100**, 503–546.

BINKS, P. B. 2002 Particles as surfactants – similarities and differences. *Curr. Opin. Colloid Interface Sci.* **7**, 21–41.

CEBERS, A., LEMAIRE, E. & LOBRY, L. 2002 Electrohydrodynamic instabilities and orientation of dielectric ellipsoids in low-conducting fluids. *Phys. Rev.* E **63**, 016301.

CERDA, E. & MAHADEVAN, L. 2003 Geometry and physics of wrinkling. *Phys. Rev. Lett.* **90**, 074302.

DOLINSKY, Y. & ELPERIN, T. 2009 Electrorotation of a leaky dielectric spheroid immersed in a viscous fluid. *Phys. Rev.* E **80**, 066607.

DOMMERSNES, P., ROZYNEK, Z., MIKKELSEN, A., CASTBERG, R., KJERSTAD, K., HERSVIK, K. & FOSSUM, J. 2013 Active structuring of colloidal armor on liquid drops. *Nat. Commun.* **4**, 2066.

FINKEN, R. & SEIFERT, U. 2006 Wrinkling of microcapsules in shear flow. *J. Phys.: Condens. Matter* **18**, L185–L191.

HA, J. W. & YANG, S. M. 2000 Electrohydrodynamics and electrorotation of a drop with fluid less conductive than that of the ambient fluid. *Phys. Fluids* **12**, 764–772.

HE, H., SALIPANTE, P. F. & VLAHOVSKA, P. M. 2013 Electrorotation of a viscous droplet in a uniform direct current electric field. *Phys. Fluids* **25**, 032106.

JONES, T. B. 1984 Quincke rotation of spheres. *IEEE Trans. Ind. Applic.* **20**, 845–849.

LAC, E. & HOMSY, G. M. 2007 Axisymmetric deformation and stability of a viscous drop in a steady electric field. *J. Fluid Mech.* **590**, 239–264.

NUDURUPATI, S., JANJUA, M., AUBRY, N. & SINGH, P. 2008 Concentrating particles on drop surfaces using external electric fields. *Electrophoresis* **29**, 1164–1172.

NUDURUPATI, S., JANJUA, M., SINGH, P. & AUBRY, N. 2009 Electrohydrodynamic removal of particles from drop surfaces. *Phys. Rev.* E **80**, 010402R.

NUDURUPATI, S., JANJUA, M., SINGH, P. & AUBRY, N. 2010 Effect of parameters on redistribution and removal of particles from drop surfaces. *Soft Matt.* **6**, 1157–1169.

PLANCHETTE, C., LORENCEAU, E. & BIANCE, A.-L. 2012 Surface wave on a particle raft. *Soft Matt.* **8**, 2444–2451.

POCIVAVSEK, L., FREY, S. L., KRISHAN, K., GAVRILOV, K., RUCHALA, P., WARING, A. J., WALTHER, F. J., DENNIN, M., WITTEN, T. A. & LEE, K. Y. C. 2008 Lateral stress relaxation and collapse in lipid monolayers. *Soft Matt.* **4**, 2019–2029.

SALIPANTE, P. F. & VLAHOVSKA, P. M. 2010 Electrohydrodynamics of drops in strong uniform dc electric fields. *Phys. Fluids* **22**, 112110.

SALIPANTE, P. F. & VLAHOVSKA, P. M. 2013 Electrohydrodynamic rotations of a viscous drop. *Phys. Rev.* E **88**, 043003.

SATO, H., KAJI, N., MOCHIZUKI, T. & MORI, Y. H. 2006 Behavior of oblately deformed droplets in an immiscible dielectric liquid under a steady and uniform electric field. *Phys. Fluids* **18**, 127101.

TAYLOR, G. I. 1966 Studies in electrohydrodynamics. I. Circulation produced in a drop by an electric field. *Proc. R. Soc. Lond.* A **291**, 159–166.

VELLA, D., AUSSILLOUS, P. & MAHADEVAN, L. 2004 Elasticity of an interfacial particle raft. *Europhys. Lett.* **68**, 212–218.

https://doi.org/10.1017/jfm.2014.289 Published online by Cambridge University Press